Measurement and systematic analysis of the cross sections of the ^{82}Kr(n, p)^{82}Br reaction induced by d-T neutrons*

Junhua Luo (罗均华)[1,2†] Long He (贺龙)[1,3] Li Jiang (蒋励)[4]

[1]Institute of New Energy, Hexi University, Zhangye 734000, China
[2]Department of Basic Science, Lanzhou Institute of Technology, Lanzhou 730050, China
[3]School of Physics and Electromechanical Engineering, Hexi University, Zhangye 734000, China
[4]Institute of Nuclear Physics and Chemistry, China Academy of Engineering Physics, Mianyang 621900, China

Abstract: The cross section of the ^{82}Kr(n, p)^{82}Br reaction induced by d-T neutrons was measured using the activation method. Incident neutrons are generated through the ^{3}H(d, n)^{4}He reaction. High-purity natural krypton gas held at high pressure was used as the target sample. The neutron energy and its uncertainty were determined based on the Q-value equation of the ^{3}H(d, n)^{4}He reaction and the experimental conditions. The neutron fluence incident on the sample is monitored by the ^{27}Al(n, α)^{24}Na reaction. The eight characteristic gamma rays of the ^{82}Br daughter nucleus were selected to determine its activity by off-line gamma spectrometry using an HPGe detector. The ^{82}Kr(n, p)^{82}Br reaction cross sections with lower uncertainties were finally determined at five neutron energies by the weighted method. The measured cross sections were compared with previous experimental studies, theoretical values from Talys-2.0, calculation results from the systematics (empirical and semi-empirical) formulas, and evaluation results. The present high-precision cross sections for the ^{82}Kr(n, p)^{82}Br reaction over a wide energy range not only help to validate and evaluate nuclear reaction models, but also substantially enrich the neutron-induced nuclear reaction cross sections database.

Keywords: Krypton-82, activation method, (n, p) reaction, cross section, systematics.

DOI: 10.1088/1674-1137/ae3601 **CSTR:** 32044.14.ChinesePhysicsC.50044001

I. INTRODUCTION

The neutron-induced nuclear reaction cross section plays a crucial role in nuclear weapon verification, medical isotope production, nuclear reaction model validation, and a variety of nuclear technology applications [1−5]. For this reason, neutron-induced cross sections of various isotopes have been measured since the mid-20th century [6−11]. In addition, specialized databases such as EXFOR have been established to collect and evaluate experimental data, providing valuable references for relevant scientific investigations [12]. Nevertheless, it does not fully meet the demand for cross-sectional data across various applications. This deficiency is primarily manifested in two aspects [13]. Several krypton reactions have proven challenging to measure due to specific experimental constraints. The first aspect is that the ^{78}Kr(n, p)^{78}Br reaction is hindered by a target isotope, which has a low abundance of 0.355% and a short product half-life of 6.45 min. Similarly, the ^{83}Kr(n, p)^{83}Br reaction is limited by the extremely low intensity of its 529.589 keV characteristic γ ray, which is only 0.013. Finally, the ^{86}Kr(n, $2n$)^{85g}Kr reaction remains challenging because the product half-life is excessively long at 10.752 years, and the strongest γ-ray at 513.997 keV has a negligible intensity of 0.0043. The second aspect is that some reactions that have not been thoroughly investigated often give low-accuracy measurements over limited energy ranges. For instance, the neutron-induced reaction ^{82}Kr(n, p)^{82}Br demonstrates this problem. For reactions without measured cross sections, possible reasons include difficulty in target preparation, insufficient decay data of the generated nuclei, or that the cross section of the reaction itself is very small and cannot be measured using the current experimental setups. For reaction ^{82}Kr(n, p)^{82}Br, only one laboratory measured the cross-section at one energy (14.4 MeV) using a natural abundance solid-state target made from powders of the inert gas quinol-clathrate: $[C_6H_4(OH)_2]_3$-0.895Kr in the early stage, with an uncertainty of 17% [14]. Kondaiah *et al*. [14] determined the cross-section of the ^{82}Kr(n, p)^{82}Br reaction using the 554 keV and 777 keV energies emitted by the residual ^{82}Br nucleus, which is 23 ± 4 mb at 14.4 ± 0.3 MeV. However,

Received 8 December 2025; Accepted 5 January 2026; Accepted manuscript online 6 January 2026

* Supported by the National Natural Science Foundation of China (12375295, 12165006)

† E-mail: luojh71@163.com

by observing the decay scheme of the ^{82}Br isotope, we found that, in order to effectively reduce the uncertainty of the cross-section, six less intense rays can be used to determine its activity (see Fig. 1).

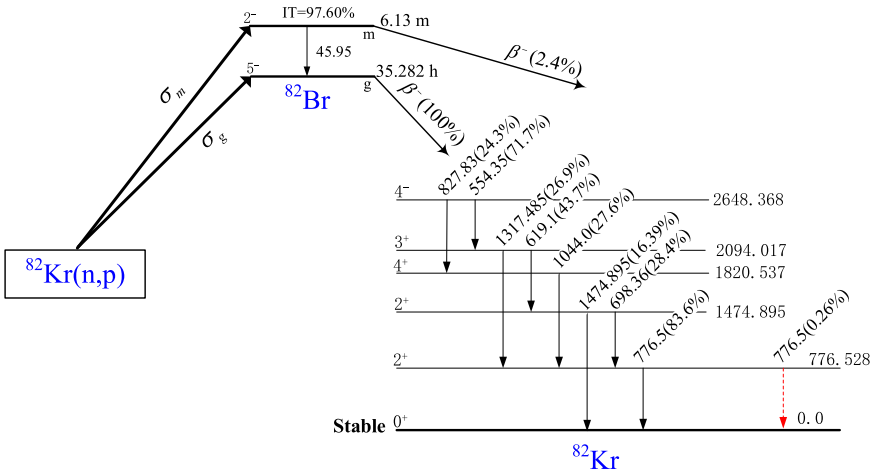

Fig. 1. (color online) The decay scheme of the radioactive nuclide ^{82m,g}Br [15], with the unit of energy in keV. The red dotted lines originate from the excited state, while the continuous black lines come from the ground state.

In order to measure the cross-section of the ^{82}Kr(n, p)^{82}Br reaction, a high-purity and high-pressure natural krypton gas target is used. The activity of the residual nucleus ^{82}Br is determined by selecting its eight characteristic rays. The uncertainty of the result is effectively reduced using the weighted average method. The measured cross sections are compared to previous experimental results [14], the results of the theoretical program Talys-2.0 [16], the results of systematic calculations [17−28], and the evaluation results of ENDF/B-VIII.1 [29], BROND-3.1 [30], JEFF- 3.3 [31], JENDL-5 [32], and TENDL-2023 [33].

II. EXPERIMENTAL PROCESS

A. Target material

Natural krypton gas has six stable isotopes, in order of abundance: ^{78}Kr (0.355%), ^{80}Kr (2.286%), ^{83}Kr (11.500%), ^{82}Kr (11.593%), ^{86}Kr (17.279%), and ^{84}Kr (56.987%) [34]. The sample container is a stainless steel spherical vessel with an inner diameter of 20 mm and a wall thickness of 1 mm that can withstand a pressure of 200 atm. Under low-temperature conditions, 99.9% pure natural krypton gas was filled into five stainless steel containers of the above-mentioned size and sealed (see Fig. 2). Under normal temperature conditions, the gas in the container is in a uniformly distributed gas-liquid mixed state [35]. During the experimental period (76 days), the mass change rate of the sample was less than 0.16%. After the experiment, the mass of the gas was obtained by subtracting the mass of the container from the total mass. Finally, it was determined that each sample had an average mass of 1.356±0.003 g.

B. Irradiation and neutron sources

The samples were irradiated using the K-400 intense neutron generator at the China Academy of Engineering Physics (CAEP). The neutrons of required energy are generated by the reaction ^{3}H(d, n)^{4}He. The new T-Ti target used in the generator had a thickness of 2.6 mg/cm^2 and an atom ratio of 1.7. The deuterium beam has an average energy of 135 keV and a beam current of 240 μA. The neutron yield was approximately (4−5)×10^{10} n/s. The samples were arranged in the form of ZrNbAl-^{nat}Kr-Al-NbZr (see Fig. 3) at the angles of 135°, 110°, 90°, 45°, and 0° relative to the incident deuterium beam, 50 mm away from the T-Ti target. To reduce the influence of low-energy scattered neutrons, the sample group was wrapped in a cadmium sheet of 99.95% purity and 1.0 mm thickness. Al, Nb, and Zr are metal circular discs with a radius of 10 mm. Their purity are 99.99%, 99.99%, and 99.5%, and their thicknesses are 0.3 mm, 0.4 mm, and 0.3 mm, respectively. Al is used to monitor

Fig. 2. (color online) Photograph of the stainless steel spherical samples used in this experiment.

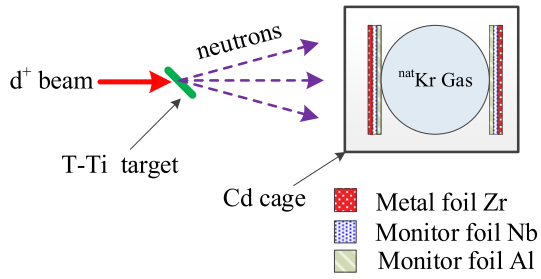

Fig. 3. (color online) Assembly diagram and relative position of sample group.

neutron fluence through reaction ^{27}Al(n, α)^{24}Na, while Nb and Zr are employed to determine neutron energy. The above-mentioned sample group was continuously irradiated by neutrons for 2 hours. The fluctuations of neutron fluence are detected by Au-Si surface barrier detectors for correction.

C. Determination of neutron energy

The energy of the neutron is determined using the Q-value equation of reaction ^{3}H(d, n)^{4}He in combination with the position of the sample relative to the direction of the incident deuterium beam. The uncertainty of energy is determined by integrating the distance from the sample to the target and the size of the sample [36]. The neutron energies and their uncertainties obtained at angles of 135, 110, 90, 45, and 0 degrees are 13.59±0.12, 13.86±0.15, 14.13±0.16, 14.70±0.13, and 14.94±0.02 MeV, respectively. For the ^{90}Zr(n, 2n)$^{89m+g}$Zr and ^{93}Nb(n, 2n)^{92m}Nb reactions, the results obtained from the cross-section ratio method [37] and the neutron energy method applied to a large sample d-T reaction data [38] are in agreement with the aforementioned results within the associated uncertainties.

D. Detector efficiency

Prior to irradiating the samples, the high-purity germanium detector (HPGe) was calibrated for detection efficiency using four standard reference sources: ^{152}Eu, ^{133}Ba, ^{137}Cs, and ^{226}Ra. The measured results were fitted with a spline function $\varepsilon(E_\gamma) = \sum_{n=0}^{5} B_n[\ln(E_\gamma)]^n$, where E_γ is the photon energy in keV. The results are presented within two confidence intervals in Fig. 4. Monte Carlo simulation was utilized to address geometric differences between the spherical sample and the standard reference source [39−41].

E. Gamma spectroscopic measurements

After activating the sample group, the radioactive nuclei ^{82}Br, ^{24}Na, $^{89m+g}$Zr, and ^{92m}Nb were measured by a HPGe detector. The detector (GEM-60P) used in the experiment has a relative efficiency of 68% and an energy resolution of 1.69 keV for the 1332 keV gamma rays of ^{60}Co. The gamma spectra were recorded by the data acquisition system (ORTEC® (GammaVision®)) [42]. A typical gamma spectrum of a natural krypton gas sample that was irradiated for 2 hours, cooled for 41.7 hours, and measured for 7.8 hours is presented in Fig. 5. The peaks of interest in the figure have been marked. The deep blue labels are from the material of the sample container (810.76 keV from ^{58}Ni(n, p)^{58}Co ($T_{1/2}$=70.86 d), 834.48 keV from ^{54}Fe(n, p)^{54}Mn ($T_{1/2}$=312.20 d), and 1377.63 keV from ^{58}Ni(n, 2n)^{57}Ni ($T_{1/2}$=35.60 h) [43]), while the black labels are selected for use in this experiment. The red-marked 606.09 keV line mainly originates from reaction ^{80}Kr(n, 2n)^{79g}Kr ($T_{1/2}$=35.04 h). The relevant parameters of the target reaction ^{82}Kr(n, p)^{82m,g}Br, and the monitored reaction ^{27}Al(n, α)^{24}Na are presented in Table 1.

F. The formula for cross sections and uncertainties

For target samples with multiple stable isotopes, there

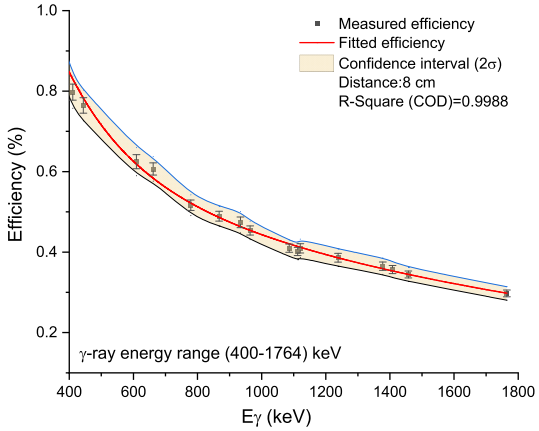

Fig. 4. (color online) Standard source calibration point and efficiency fitting curve.

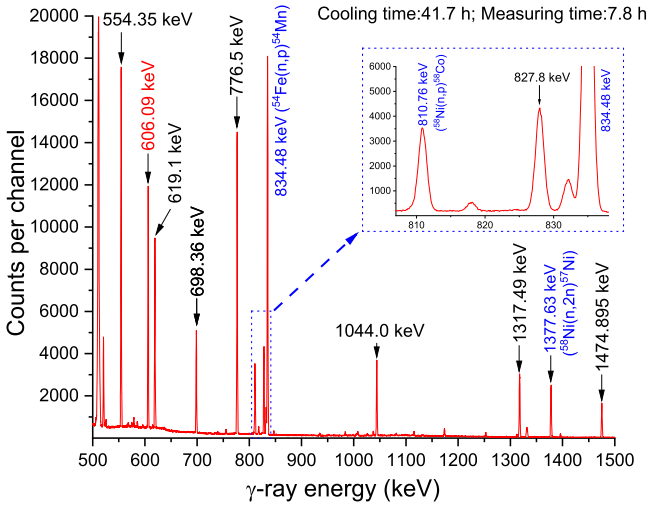

Fig. 5. (color online) The gamma spectrum of the krypton gas sample was measured after 2 hours of continuous neutron irradiation, followed by 41.7 hours of cooling, and the measurement time was 7.8 hours.

Table 1. The target nuclide abundance, threshold energy, and decay data of daughter nuclides of the measured reaction ^{82}Kr(n, p) and the supervisory reaction [15, 44].

Reaction	Abundance of target isotope (%)	Half-life of product	E-threshold/MeV	Mode of decay (%)	$E\gamma$ /keV	$I\gamma$ (%)
^{82}Kr(n, p)^{82m}Br	11.593_{31}	6.13 m_5	2.386	IT(97.60)β^- (2.40)	776.52	0.26
^{82}Kr(n, p)^{82g}Br	11.593_{31}	35.282 h_7	2.339	β^- (100)	**554.35**	**71.7$_{10}$**
					619.1	**43.7$_6$**
					698.36	**28.4$_4$**
					776.5	**83.6$_{12}$**
					827.83	**24.2$_3$**
					1044.0	**27.6$_4$**
					1317.49	**26.9$_4$**
					1474.895	**16.39$_{23}$**
^{27}Al(n, α)^{24}Na	100	14.997 h_{12}	3.249	β^-(100)	1368.6	100

The eight characteristic gamma rays used in the analysis are show in bold.

is a possibility that one residual nucleus comes from different reaction channels. In this situation, the formation cross-section can be calculated as [45, 46]:

$$\sigma_x^{\rm tot} = \frac{[S\varepsilon I_\gamma \eta KMD]_{Al}}{[S\varepsilon I_\gamma KMD]_x} \cdot \frac{[\lambda AFC]_x}{[\lambda AC]_{Al}} \sigma_{Al}. \tag{1}$$

For krypton gas, the formation cross-section of ^{82}Br is expressed as:

$$\begin{aligned}\sigma_x^{\rm tot}(^{\rm nat}{\rm Kr}(n,x)^{82}{\rm Br}) =& 0.11593\sigma(^{82}{\rm Kr}(n,p)^{82}{\rm Br}) \\ &+ 0.115\sigma(^{83}{\rm Kr}(n,d*)^{82}{\rm Br}) \\ &+ 0.56987\sigma(^{84}{\rm Kr}(n,t)^{82}{\rm Br}) \\ =& \frac{[S\varepsilon I_\gamma \eta KMD]_{Al}}{[S\varepsilon I_\gamma KMD]_x} \frac{[\lambda AFC]_x}{[\lambda AC]_{Al}} \sigma_{Al},\end{aligned} \tag{2}$$

where Al and x denote the monitored and measured reactions, respectively. F represents the overall correction factor for the activity, which can be calculated as:

$$F = f_s \times f_c \times f_g \times f_\Omega, \tag{3}$$

Where the correction factors f_s, f_c, $f_{\rm g}$, and f_Ω account for the sample's self-absorption at a particular gamma, coincidence summing effect, geometrical arrangement, and the solid angle, respectively. These correction calculation formulas refer to our earlier literature [47, 48]. Due to differences in the geometry between the monitor foil and the spherical sample, the correction factor for the solid angle of the neutron flux was determined to be f_Ω =1.076 based on the experimental conditions of this study. The geometric correction factor for the spherical sample was $f_{\rm g}$=1.174. The absorption coefficients were obtained through interpolation of the data reported in the literature [49].

III. WEIGHTED AVERAGE AND UNCERTAINTY ANALYSIS

The uncertainties of the experimental cross sections for the eight characteristic gamma rays were assessed by applying the root sum square technique [50, 51]. According to Eq. (1), the primary contributors to these uncertainties are as follows: the monitor reaction (0.39%–0.56%), counting statistics (with uncertainty values for each energy line: 554.35 keV (0.31%–4.64%), 619.1 keV (0.48%–9.60%), 698.36 keV (0.62%–9.81%), 776.5 keV (0.27%–3.04%), 827.83 keV (0.71%–12.13%), 1044.0 keV (0.59%–6.66%), 1317.49 keV (0.56%–8.62%), and 1474.895 keV (0.74%–13.00%)), detection efficiency (2.5%–3.0%), relative gamma-ray emission intensity (1.3%–1.4%), half-life (0.02%–0.08%), sample mass (0.2%), timing accuracy (<0.1%), gamma-ray self-absorption (~0.5%), and isotope abundance (0.03%–0.27%).

A. Weighted average

By analyzing the eight characteristic gamma rays emitted from the ^{82}Br nucleus, the cross section of the ^{82}Kr(n, p) reaction can be expressed as $\sigma_i \pm \Delta\sigma_i$, with i varying from 1 to 8. To determine the weighted average cross section, the uncertainties were first normalized by inverting the square of each uncertainty, and the calculation was performed using the following expression [52]:

$$\sigma = \frac{\sum_{i=1}^{8}[\sigma_i/(\Delta\sigma_i)^2]}{\sum_{i=1}^{8}[1/(\Delta\sigma_i)^2]}, \tag{4}$$

B. Experimental standard deviation

The experimental standard deviation of the results was classified as Class A and Class B. The standard deviation $\Delta\sigma_A$ associated with Class A was determined using the following definition [52]:

$$\Delta\sigma_A = \left[\frac{\sum_{i=1}^{n}[(\sigma_i-\sigma)^2/(\Delta\sigma_i)^2]}{(n-1)\sum_{i=1}^{n}[1/(\Delta\sigma_i)^2]}\right]^{1/2}. \quad (5)$$

A major challenge in experimental research is obtaining the most reliable information from a limited number of measurements. In particular, Eq. (5), which is used to calculate the error $\Delta\sigma_A$ of the weighted average, may produce non-physical results when applied to a very small amount of data. To tackle this issue, we incorporate $\Delta\sigma_B$, which limits the impact of individual uncertainties on the overall error $\Delta\sigma$ [52]:

$$\Delta\sigma_B = \left[\sum_{i=1}^{n}\frac{1}{(\Delta\sigma_i)^2}\right]^{-1/2}. \quad (6)$$

However, Eq. (6) can still produce misleading results when two data points exhibit significant inconsistency despite having relatively small uncertainties. In these situations, the following expression can be used to more accurately estimate the standard deviation $\Delta\sigma$ of the weighted mean σ for a small dataset [52]:

$$\Delta\sigma = \max(\Delta\sigma_A, \Delta\sigma_B). \quad (7)$$

In this study, the uncertainty associated with the weighted average cross section varied between 2.61% and 2.95%. A summary of the findings is presented in Table 2.

IV. MODEL AND SYSTEMATIC CALCULATIONS

A. Model simulations with TALYS-2.0

TALYS is a sophisticated computational tool designed to analyze and predict nuclear reactions, particularly focusing on neutron-induced processes [16]. It is crucial to accurately simulate neutron-induced reaction cross sections because they are essential for applications in the fields of nuclear energy, medical isotope production, and astrophysics. TALYS integrates various nuclear reaction models, enabling comprehensive evaluations of reactions across a wide energy range, from thermal to intermediate energies [53, 54]. The theoretical framework underlying neutron-induced reaction cross section calculations in TALYS is primarily based on statistical models, particularly the Hauser-Feshbach theory. This approach enables the modeling of compound nucleus reactions, where the interaction between the incident neutron and the target nucleus leads to the formation of an intermediate compound state before decay into final products [55]. The inclusion of nuclear structure parameters, including the level density parameter, which is crucial for determining the density of available energy states in the nucleus at a given excitation energy, significantly improves the accuracy of these simulations [16]. The level density parameter is derived from the Gilbert-Cameron model, which takes into account collective effects and pairing correlations within the nucleus. This parameter is essential for calculating neutron separation energies and other related observables, as well as predicting the likelihood of various reaction channels [55]. By accurately modeling these parameters, TALYS provides reliable predictions of neutron-induced reaction cross sections, thereby advancing nuclear physics research and its practical applications.

Version 2.0 of Talys was used for the ^{82}Kr(n, p)^{82}Br reaction. Theoretical excitation functions were generated for neutron energies ranging from the reaction threshold to 20 MeV. These calculations were performed using de-

Table 2. The cross-sectional measurements for various characteristic rays, along with their calculated weighted average values.

Reaction	$E\gamma$ /keV	Cross sections (in mb) at various neutron energies (in MeV)				
		13.59±0.12	13.86±0.15	14.13±0.16	14.70±0.13	14.94±0.02
^{82}Kr(n, p)^{82}Br	554.35	20.5±1.1	21.7±1.2	23.7±1.3	25.6±1.4	27.1±1.4
	619.1	21.2±1.6	23.7±1.8	24.1±1.8	26.2±2.0	26.8±1.9
	698.36	21.6±2.3	22.8±2.5	24.5±2.8	25.3±2.7	27.6±2.6
	776.5	20.9±1.1	22.1±1.3	23.8±1.3	25.9±1.3	27.4±1.4
	827.83	23.1±2.7	23.1±2.7	23.9±2.7	26.4±2.8	28.1±2.6
	1044.0	22.2±2.6	22.0±2.5	24.4±2.7	25.5±2.8	27.3±2.9
	1317.49	21.8±2.7	22.3±2.8	23.7±3.1	24.3±3.1	27.7±3.1
	1474.895	21.3±2.8	21.8±2.8	23.1±3.1	25.5±3.2	27.2±3.0
Weighted average ± standard uncertainty		21.1±0.6	22.3±0.7	23.9±0.7	25.7±0.7	27.3±0.7
^{27}Al(n, α)^{24}Na (IRDFF-II,2020)	1368.6	125.3±0.7	123.6±0.6	120.6±0.6	112.6±0.4	109.0±0.5

fault settings, with modifications limited to the selected level density models. Additional information regarding the cascade density parameters has been documented in prior studies [36].

B. Systematic calculations

To determine the cross-section value of a specific nuclear reaction, systematic methods, combined with experimental data and theoretical computations, provide a valuable and effective strategy. The key strength of the systematics approach lies in its ability to estimate cross sections for unmeasured reactions by using experimentally observed data of related reactions. Numerous studies [17–28] have utilized available experimental results to establish various empirical and semi-empirical formulas (systematic models) for predicting cross-section values at different neutron energy levels (see Table 3). An analysis of these systematic expressions reveals that the cross section is generally dependent on factors such as the asymmetry parameter $[(N\text{-}Z)/A]$ or $[(N\text{-}Z+1)/A]$, the atomic mass number A, and the incident neutron energy E_n. The reaction cross section that depends on the aforementioned factors can be expressed as follows:

$$\sigma_{n,p} = f[E_n, A^{1/3}, (N-Z)/A]. \tag{8}$$

Current systematic formulas are generally based on statistical models designed for specific neutron energy levels, such as 14.5 MeV. In these formulations, the cross section for compound nucleus formation is primarily influenced by the mass number A of the target nucleus. Additionally, the influence of the Q-value is associated with the proton and neutron counts within the target nucleus.

V. RESULTS AND DISCUSSION

The production of radioactive nuclide ^{82}Br using natural krypton isotopes as targets has three pathways: ^{82}Kr(n, p)^{82}Br (E_{th}=2.339 MeV), ^{83}Kr(n, d)^{82}Br (E_{th}=7.648 MeV), and ^{84}Kr(n, t)^{82}Br (E_{th}=11.961 MeV). The activation method cannot distinguish the respective contributions of the three paths to the ^{82}Br counts. However, through theoretical calculations by Talys-2.0, it was found that the cross-section of the ^{84}Kr(n, t)^{82}Br reaction at the neutron energy of 14 MeV is less than 0.001 mb (and thus is ignored), while the cross-sections of the ^{83}Kr(n, d)^{82}Br reaction at neutron energies of 13.59±0.12, 13.86±0.15, 14.13±0.16, 14.70±0.13, and 14.94±0.02 MeV are 0.82, 1.64, 1.86, 4.45, and 4.90 mb, respectively (and are deducted using Formula 2). In this experiment, eight gamma-rays with energies of 554.35 keV (I_γ=71.7%), 619.1 keV (I_γ=43.7%), 698.36 keV (I_γ=28.4%), 776.5 keV (I_γ=83.6%), 827.83 keV (I_γ=24.2%), 1044.0 keV (I_γ=27.6%), 1317.49 keV (I_γ=26.9%), and 1474.895 keV (I_γ=16.39%) emitted ^{82}Br decay were used to measure the cross section of the ^{82}Kr(n, p)^{82}Br reaction (E_{th}= 2.339 MeV). The strong gamma line at 606.09 keV shown in Fig. 5 cannot be used to determine the activity of ^{82}Br because it mainly originates from the product nucleus ^{79g}Kr ($T_{1/2}$=35.04 h, I_γ=8.1%) of the reaction ^{80}Kr(n,

Table 3. Comparative analysis of (n, p) reaction cross-section systematics at a neutron energy of 14.5 MeV.

Author	Formula, σ /mb	Mass region
Levkovski [17]	$\sigma_{n,p} = 50.21(A^{1/3}+1)^2 \exp(-33.80(N-Z)/A)$	$40 \leqslant A \leqslant 209$
Forrest [18]	$\sigma_{n,p} = 900(A^{1/3}+1)^2 \exp(-49.27(N-Z)/A + 197.1(N-Z)^2/A^2 - 0.45A^{1/2})$	$40 \leqslant A \leqslant 187$
Ait-Tahar [19]	$\sigma_{n,p} = 90.68(A^{1/3}+1)^2 \exp(-34.48(N-Z+1)/A)$	$40 \leqslant A \leqslant 187$
Broeders and Konobeyev [20]	$\sigma_{n,p} = 53.093(A^{1/3}+1)^2 \exp(A^{0.5}(-4.4785(N-Z+1)/A + 0.047174Z/A^{1/3} - 0.27407))$	$Z \leqslant 50$
	$\sigma_{n,p} = 53.093(A^{1/3}+1)^2 A^{0.75718}(-0.61348(N-Z+1)/A + 0.1511)^3$	$Z > 50$
Kasugai *et al*. [21]	$\sigma_{n,g} = 1264(N-Z+1)\exp(-46.63(N-Z+1)/A)$	$28 \leqslant A \leqslant 187$
Doczi *et al*. [22]	$\sigma_{n,q} = 18.12\left(A^{1/5}+1\right)^2 \exp\left(-19.16\left((N-Z)/A + (N-Z)^2/A^2\right)\right.$	$28 \leqslant A \leqslant 209$
Bychkov [23]	$\sigma_{n,p} = 42.807(A^{1/3}+1)^2 \exp((A/145)^{0.5}(-50.385(N-Z+1)/A + 0.58916(Z-1)/A^{1/3} - 3.2374))$	
Konobeyev and Korovin [24]	$\sigma_{n,p} = 53.093(A^{1/3}+1)^2(A^{1.1128}(1.1242S^2 - 0.73212S + 0.11707)^3$ $+0.4936\exp(-194.69S^2 - 5.3778S))$ $\quad S = (N-Z+1)/A$	
Habbani *et al*. [25]	$\sigma_{n,p} = 60.34(A^{1/3}+1)^2 \exp(-34.44(N-Z+1)/A)$	$28 \leqslant A \leqslant 208$ (even-A)
	$\sigma_{n,p} = 20.91(A^{1/3}+1)^2 \exp(-29.53(N-Z)/A)$	$29 \leqslant A \leqslant 209$ (odd-A)
Luo *et al*. [26]	$\sigma_{n,p} = 62.98(A^{1/3}+1)^2 \exp(-34.45(N-Z)/A)$	$46 \leqslant A \leqslant 196$
Akash Hingu *et al*. [27]	$\sigma_{n,p} = 15.32(A^{1/3}+1)^2 \exp(-26.73(N-Z)/A + 44.19(N-Z)^2/A^2)$	$24 \leqslant A \leqslant 103$ (for $Z \leqslant 50$)
	$\sigma_{n,p} = 1.67(A^{1/3}+1)^2 \exp(2.158(N-Z)/A - 93.13(N-Z)^2/A^2)$	$108 \leqslant A \leqslant 238$ (for $Z > 50$)
Dashty *et al*. [28]	$\sigma_{n,p} = 16.125Z^{1.4704} \exp(-40.25(N-Z)/A)$	$44 \leqslant A \leqslant 206$ (Even-Even)
	$\sigma_{n,p} = 8.7841 \cdot Z^{1.457} \cdot \exp(-34.3(N-Z)/A)$	$45 \leqslant A \leqslant 211$ (Even-Odd)
	$\sigma_{n,p} = 39.568 \cdot Z^{0.845} \cdot \exp(-27.855(N-Z)/A)$	$49 \leqslant A \leqslant 205$ (Odd-Even)
	$\sigma_{n,p} = 192.85 \cdot Z^{0.377} \cdot \exp(-23.455(N-Z)/A)$	$100 \leqslant A \leqslant 212$ (Odd-Odd)

2n), not only from ^{82}Br (I_γ=1.2299%). The ^{27}Al(n, α)^{24}Na (E_{th}=3.249 MeV) reaction was selected as the standard reaction to monitor the neutron flux. In earlier experiments [14], the cross section of ^{82}Kr(n, p)^{82}Br reaction was measured using the 554.35 keV (I_γ=71.7%) and 776.5 keV (I_γ=83.6%) characteristic gamma rays, along with the ^{27}Al(n, α)^{24}Na (E_{th}=3.249 MeV) and ^{56}Fe(n, p)^{56}Mn (E_{th}=2.966 MeV) reference reactions. At a neutron energy of 14.4 ± 0.3 MeV, a value of (23 ± 4) mb was obtained, with an uncertainty of 17.4%. The application of the weighted average method reduced the uncertainty in the ^{82}Kr(n, p)^{82}Br cross section to less than 3.0%. The measured cross sections and systematic calculation results are listed in Table 4. The final correlation matrix for the ^{82}Kr(n, p)^{82}Br reaction cross-section is presented in Table 5. All experimental data, TALYS-2.0 theoretical calculation results, and systematic results are presented in Fig. 6. Additionally, the experimental results, systematic results, and evaluation curves from databases [29−33] are shown in Fig. 7. To compare various results, $\chi^2 = \frac{1}{N}\sum_{i=1}^{N}[(\sigma_i^{calc}-\sigma_i^{exp})/(k\Delta\sigma_i^{exp})]^2$ values are calculated [36]. The results are provided in Tables 6 and 7. As shown in Fig. 6, our experimental data in the energy interval of 13 to 15 MeV are in good agreement with earlier experimental results [14], as well as systematic data from Levkovski [17], Bychkov *et al*. [23], Konobeyev *et al*. [24], and Dashty [28]. Additionally, our findings are consistent with the TALYS-2.0 theoretical predictions based on ldmodel 1 within the uncertainty bounds (see Table 6). Nevertheless, when using ldmodels 2-6, our results are lower than those of TALYS-2.0 calculations. This conclusion indicates that the Constant Temperature +

Table 4. Experimental cross-section data and systematic results for the ^{82}Kr(n, p)^{82}Br reaction at associated neutron energies.

References	E_n /MeV	Cross sections /mb
Present experimental results	13.59±0.12	21.1±0.6
	13.86±0.15	22.3±0.7
	14.13±0.16	23.9±0.7
	14.70±0.13	25.7±0.7
	14.94±0.02	27.3±0.7
Kondaiah et *al*. [14]	14.4±0.3	23±4
Systematic result		
Levkovski [17]	14.5	23.3
Forrest [18]	14.5	20.1
Ait-Tahar [19]	14.5	25.4
Broeders and Konobeyev [20]	14.5	19.0
Kasugai *et al*. [21]	14.5	26.7
Doczi *et al*. [22]	14.5	48.1
Bychkov *et al*. [23]	14.5	23.6
Konobeyev and Korovin [24]	14.5	23.2
Habbani *et al*. [25]	14.5	17.0
Luo *et al*. [26]	14.5	26.9
Akash Hingu *et al*. [27]	14.5	32.4
Dashty *et al*. [28]	14.5	23.1

Table 5. Measured cross sections of the ^{82}Kr(n, p)^{82}Br reaction, total uncertainties, and correlation matrices.

Neutron energy E_n /MeV	Cross section σ_x /mb	$\Delta\sigma_x$(%)	Correlation matrix				
13.59±0.12	21.1±0.6	2.90	1.000				
13.86±0.15	22.3±0.7	2.95	0.296	1.000			
14.13±0.16	23.9±0.7	2.87	0.293	0.295	1.000		
14.70±0.13	25.7±0.7	2.82	0.295	0.297	0.294	1.000	
14.94±0.02	27.3±0.7	2.61	0.298	0.300	0.297	0.299	1.000

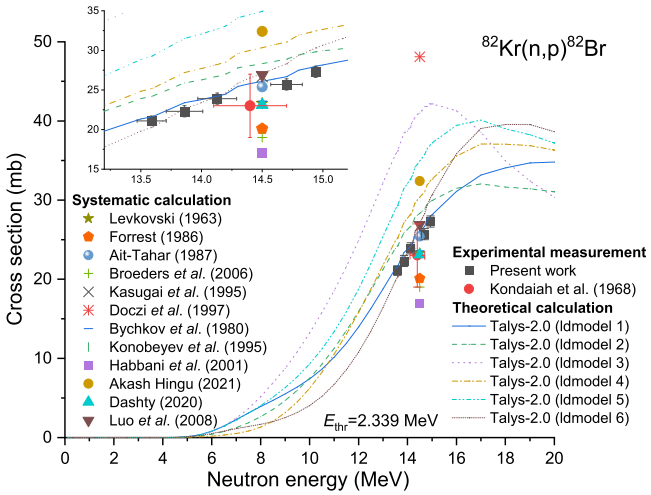

Fig. 6. (color online) Theoretical excitation function for the ^{82}Kr(n, p)^{82}Br reaction, along with experimental data and systematic results.

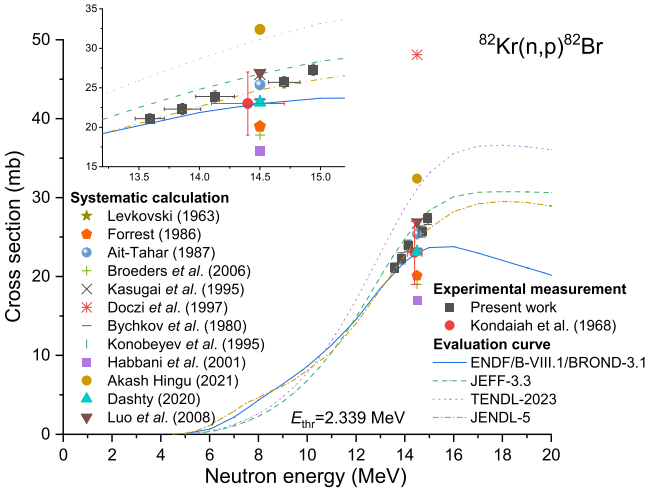

Fig. 7. (color online) Experimental data, systematic results, and evaluated curves for the ^{82}Kr(n, p)^{82}Br reaction.

Table 6. A comparison of the experimentally obtained cross-section values with the theoretical predictions from TALYS-2.0 for different level density models, under a coverage factor of k=2 and a 95% confidence interval.

Reaction	χ^2 (k=2, P=95%)					
	ldmodel 1	ldmodel 2	ldmodel 3	ldmodel 4	ldmodel 5	ldmodel 6
^{82}Kr(n, p)^{82}Br	**0.313**	5.134	131.924	12.319	45.772	1.733

The smallest value is highlighted in bold.

Table 7. A comparison of the experimentally determined cross-section to the evaluated values, under a coverage factor of k=2 and a 95% confidence level. The ENDF/B-VIII.1 dataset is consistent with BROND-3.1.

Reaction	χ^2 (k=2, P=95%)			
	ENDF/B-VIII.1 (BROND-3.1)	JEFF-3.3	JENDL-5	TENDL-2023
^{82}Kr(n, p)^{82}Br	2.454	1.382	**0.276**	17.245

The smallest value is highlighted in bold.

Fermi Gas model (CTM), which corresponds to ldmodel 1, is sufficiently accurate for describing the ^{82}Kr(n, p)^{82}Br reaction. Furthermore, as depicted in Fig. 7, our measurements within the neutron energy range of 13-14.7 MeV are also consistent with the JENDL-5 evaluation curve [32] (see Table 7). It is worth noting that when the energy exceeds 14 MeV, the evaluation results of ENDF/B-VIII.1 [29] (BROND-3.1 [30]) and TENDL-2023 [33] differ significantly.

VI. CONCLUSION

The activation cross sections for the ^{82}Kr(n, p)^{82}Br reaction were determined at neutron energies of 13.59±0.12, 13.86±0.15, 14.13±0.16, 14.70±0.13, and 14.94±0.02 MeV utilizing updated decay parameters. The activity of the produced radionuclides was determined by measuring eight distinct gamma-ray emissions from ^{82}Br. The contributions of the interfering ^{83}Kr(n, d)^{82}Br reaction were carefully subtracted. A weighted average approach was employed to improve the measurement precision, achieving an overall uncertainty of less than 3%. In contrast to previous studies, the present dataset covers a wider range of neutron energies. Theoretical cross sections for the ^{82}Kr(n, p)^{82}Br reaction were calculated using the TALYS-2.0 software with different level density models. The experimental findings of this study were compared to previous experimental data, theoretical predictions from various models, evaluated data, and results from systematic formulas. Nuclear model simulations performed with the TALYS code revealed that the Constant Temperature + Fermi Gas model (CTM) (ldmodel 1) best describes the cross-section behavior of the ^{82}Kr(n, p)^{82}Br reaction. These findings have far-reaching implications for improving nuclear data repositories, validating reaction models, and facilitating real-world applications. Furthermore, the high-accuracy cross-section measurements offer valuable input for refining parameters in systematic formulas used for (n, p) reactions.

ACKNOWLEDGEMENTS

We would like to thank the Intense Neutron Generator group at Chinese Academy of Engineering Physics for performing the irradiations.

References

[1] W. Tornow, S. W. Finch, and Yuko Saito, Phys. Rev. C **112**, 014615 (2025)
[2] B. Li *et al*., Chin. Phys. C **48**, 104002 (2024)
[3] S. M. Qaim, Nucl. Med. Biol. **44**, 31 (2017)
[4] L. He, J. Luo, and L. Jiang, Chin. Phys. C, **47**, 034001 (2023)
[5] J. Luo, L. He, L. Zhou *et al*., Chin. Phys. C **48**, 124001 (2024)
[6] S. M. Qaim, Nucl. Phys. A **458**, 237 (1986)
[7] J. Zeng *et al*., Nucl. Phys. A **1030**, 122569 (2023)
[8] A. Gandhi *et al*., Chin. Phys. C **46**, 014002 (2022)
[9] Bhargav Soni *et al*., Eur. Phys. J. Plus **135**, 300 (2020)
[10] J. Luo *et al*., Nucl. Sci. Tech. **34**, 4 (2023)
[11] J. Luo, L. He, and L. Jiang, Radia. Phys. Chem. **238**, 113146 (2026)
[12] EXFOR, IAEA experimental nuclear reaction data (EXFOR) Brookhaven National Laboratory, National nuclear data center (2022) https://www-nds.iaea.org/exfor/exfor.htm.
[13] J. Luo, *14 MeV Neutron Physics and Cross Section Measurement* (Science Press, Beijing, 2021) (in Chinese)
[14] E. Kondaiah, N. Ranakumar, and R. W. Fink, Nucl. Phys. A, **120**, 337 (1968)
[15] J. K. Tuli and E. Browne, Nucl. Data Sheets **157**, 260 (2019)
[16] A. Koning, S. Hilaire, and S. Goriely, Eur. Phys. A **59**, 131 (2023)

[17] V. N. Levkovski, Zh. Eksp. Teor. Fiz. **45**, 305 (1963)
[18] R. A. Forrest, AERE-R 12419 (Harwell Laboratory, 1986)
[19] S. Ait-Tahar, Nucl. Phys. **13**, 121 (1987)
[20] C. H. M. Broeders and A. Yu. Konobeyev, Nucl. Phys. A **780**, 130 (2006)
[21] Y. Kasugai *et al.* , JAERI-Conf. 95-008, 1995
[22] R. Doczi *et al*., INDC(HUN)-032, NDS, IAEA, 1997
[23] V. M. Bychkov *et al.* , IAEA INDC(CCP) 146/U, 1, 1980
[24] A. Yu. Konobeyev and Yu. A. Korovin, Nucl. Instrum. Meth. B **103**, 15 (1995)
[25] F. I. Habbani and Khalda T. Osman, Appl. Radia. Isoto. **54**, 283 (2001)
[26] J. Luo, F. Tuo, F. Zhou *et al*., Nucl. Instrum. Meth. B **266**, 4862 (2008)
[27] Akash Hingu *et al*., Radiat. Phys. Chem. **188**, 109634 (2021)
[28] Dashty T. Akrawy *et al*., Int. J. Mod. Phys. E **29**, 2050052 (2020)
[29] D. A. Brown *et al*., Nucl. Data Sheets **148**, 1 (2018)
[30] A. I. Blokhin *et al*., Vopr. At. Nauki Tekh. Ser. Yad. Konstanty **2**, 62 (2016)
[31] A. J. M. Plompen *et al*., Eur. Phys. A **56**, 181 (2020)
[32] O. Iwamoto *et al*., J. Nucl. Sci. Technol. **60**, 1 (2023)
[33] A. J. Koning *et al*., Nucl. Data Sheets **155**, 1 (2019)
[34] ENSDF, 2025. (Evaluated Nuclear Structure Data File), (Last updated 2025-8-07) https://www.nndc.bnl.gov/nudat3/
[35] G. Rupp *et al*., Nucl. Instrum. Meth. A **608**, 152 (2009)
[36] J. Luo, L. He, L. Zhou *et al*., Eur. Phys. A **61**, 30 (2025)
[37] V. E. Lewis and K. J. Zieba, Nucl. Instrum. Meth. **174**, 141 (1980)
[38] J. Luo, L. Du, and J. Zhao, Nucl. Instrum. Meth. B **298**, 61 (2013)
[39] J. Mayer *et al*., Nucl. Instrum. Meth. A **972**, 164102 (2020)
[40] M. Omer *et al*., Radtat. Phys. Chem. **198**, 110241 (2022)
[41] A. Subercaze *et al*., Nucl. Instrum. Meth. A **1039**, 167096 (2022)
[42] GammaVision®-32, *Gamma-Ray Spectrum Analysis and MCA Emulator*, Software User's Manual, Software Version 5.3
[43] NuDat-3, https://www.nndc.bnl.gov/nudat3/
[44] M. Shamsuzzoha Basunia and Anagha Chakraborty, Nucl. Data Sheets **186**, 3 (2022)
[45] J. Luo, L. He, L. Zhou *et al*., Radiat. Phys. Chem. **227**, 112384 (2025)
[46] J. Luo *et al*., Chin. Phys. C **46**, 044001 (2022)
[47] J. Luo *et al*., Eur. Phys. A **58**, 142 (2022)
[48] F. Zhou, Y. Zhang, J. Luo *et al*., HEP & NP **31**, 487 (2007) (in Chinese)
[49] J. H. Hubbell and S. M. Seltzer, *Tables of x-ray mass attenuation coefficients and mass energy-absorption coefficients from 1 keV to 20 MeV for elements Z = 1 to 92 and 48 additional substances of dosimetric interest* (2004) http://physics.nist.gov/PhysRefData/XrayMassCoef/tab3.html.
[50] N. Otuka *et al*., Radiat. Phys. Chem. **140**, 502 (2017)
[51] D. L. Smith and N. Otuka, Nucl. Data Sheets **113**, 3006 (2012)
[52] J. Luo, L. He, L. Zhou *et al*., Chin. Phys. C **49**, 084005 (2025)
[53] S. Hoblit *et al*., Nucl. Data Sheets **112**, 3075 (2011)
[54] K. Blaum and M. J. G. Borge, Eur. Phys. A **60**, 94 (2024)
[55] Georg Schnabel, Jeju, Korea, April 16-20, 2017, on USB (2017)